Dependence of the electron-inelastic-scattering rate on disorder and temperature in a strongly disordered superconductor

Deuk Soo Pyun and Thomas R. Lemberger
Department of Physics, Ohio State University, Columbus, Ohio 43210
(Received 21 February 1991)

The electron-inelastic-scattering rate, $1/\tau_{in}$, is studied in superconducting amorphous-composite indium oxide films over substantial ranges of resistivity $\rho_{4.2}$ ($1.4 \le \rho_{4.2} \le 9.8$ mΩ cm), sheet resistance $R_\square$ ($0.17 \le R_\square \le 1.8$ kΩ), and reduced temperature T/T_{co} ($0.17 \le T/T_{co} \le 0.6$), using an electron tunneling technique. $1/\tau_{in}(T)$ is obtained by a phenomenological analysis of the data. The main result is that $1/\tau_{in} \approx 2.8 \times 10^{10}\ s^{-1}[\rho_{4.2}\ (m\Omega\ cm)\ T_{co}\ (K)]^{3/2}(T/T_{co})^3$. That $1/\tau_{in} \propto \rho_{4.2}^{3/2}$, as opposed to $1/\tau_{in} \propto R_\square$, indicates the films are three dimensional (3D) rather than 2D for inelastic scattering. A recent theory explains this result as inelastic electron-phonon scattering that is enhanced by disorder that is strong enough to suppress the normal-state density of states at the Fermi energy significantly.

I. INTRODUCTION

In a previous paper,[1] tunneling measurements of the inelastic-scattering rate $1/\tau_{in}(T)$ in amorphous-composite indium oxide films (a-InO_x) found $1/\tau_{in} \propto (T/T_{co})^3$ even at low reduced temperatures, $T/T_{co} \approx 0.17$, where $1/\tau_{in} \ll$ the order parameter $\Delta/\hbar$ so that it is a small perturbation. This result was surprising since the dominant inelastic-scattering process was expected to be electron-electron scattering, which was predicted to be proportional to $\exp(-\Delta/kT)$ at low temperatures $T \ll T_{co}$.[2] A measurement of quasiparticle relaxation times in weakly disordered 2D Al films was consistent with this rapid decrease.[3]

Reference 1 discusses numerous measurements[4-8] of $1/\tau_{in}$ in the normal state and at or just below T_{co}, which, in agreement with theory,[9-12] demonstrate that disorder enhances electron-electron scattering while it reduces electron-phonon scattering in the normal state. Theory of electron-electron and electron-phonon scattering in superconductors has been discussed recently by Devereaux and Belitz.[15] The basic picture is that in weakly disordered superconductors, such as amorphous 3D Pb-Bi, the electron-phonon scattering rate, as opposed to the recombination rate due to phonon emission, is proportional to $(T/\Delta)^{9/2}$, and all other electron-phonon and electron-electron processes are exponentially small at low temperatures. However, because of the small coherence factor for scattering of quasiparticles at $E=\Delta$ to other states near $E=\Delta$, the electron-phonon scattering rate is so much smaller than the recombination rate near T_{co} that it becomes larger than the recombination rate only at very low temperatures where both are too small to observe. In somewhat more disordered conductors, the electron-phonon coupling decreases as the electron mean free path decreases below the wavelength of a typical thermal phonon, while electron-electron scattering increases due to the reduction in screening of the Coulomb interaction between electrons, as first discussed by Schmid.[13] Thus, we expected electron-electron scattering to dominate in our experiment.

Very recently, Devereaux and Belitz[14,15] have found that for very disordered superconductors, the reduction in screening of Coulomb interactions increases electron-phonon coupling and modifies quasiparticle states enough to remove the coherence factor bottleneck for electron-phonon scattering. These effects are concurrent with a substantial reduction in the normal-state density of states at the Fermi level due to increased electron-electron interactions.[12] Our a-InO_x films show this large suppression.[16] For $T/T_{co} \ll 1$, they calculate the imaginary part of the electron self energy at $E=\Delta$, which is closely related to the inelastic scattering rate from our experiment although the exact relationship is unclear. They find that electron-phonon scattering, enhanced by disorder, has the magnitude and temperature dependence which we observe, as described below.

In the present paper, we further test the theory by extending our study to a wider range of sample disorder and film thickness than in Ref. 1. Also, more details about the properties of the a-InO_x films and about the phenomenological data analysis are presented than in Ref. 1. Even more details can be found in Ref. 17.

The idea of the experimental method is to obtain an effective rate $1/\tau_{in}$ from modifications that inelastic scattering makes in the superconducting density of states, measured via electron tunneling. The main difficulty is that disorder also makes large modifications in the energy dependence of the normal-state electron density of states, $N_n(E)$. To get the energy dependence due to superconductivity alone, we must divide out $N_n(E)$ from the density of states $N_s(E)$ measured below T_{co} where $N_n(E)$ can not be measured directly. [Critical magnetic fields are so large that they would alter $N_n(E)$.] As explained below, this division can be done with measurements of the differential conductance G_j of high-resistance superconductor-insulator-normal metal (SIN) junctions as a function of not only bias voltage and temperature, but also of supercurrent applied in the a-InO_x strip.

II. EXPERIMENTAL DETAILS

A. Sample preparation and characterization

Samples are high-resistance Al-AlO_x-InO_x tunnel junctions. Sample configuration and wiring are illustrated in Fig. 1. 2000-Å thick Al (plus 1 wt. % Mn) is deposited on a glass substrate through a mechanical mask from a thermal evaporation source and exposed to air for about 30 minutes to form the tunneling barrier. (1 wt. % Mn lowers the superconducting transition in Al to below 0.5 K, the lowest temperature available in this work.) Then 1500-Å SiO is vapor deposited to define the junction area. Finally, the a-InO_x film is deposited at room temperature on the top of oxide barrier by reactive ion sputtering in the presence of a partial pressure of oxygen.[18] The nominal junction area and normal junction resistance are 300×300 μm^2 and 0.5–1 kΩ. The junctions are very durable under many thermal cyclings, and the junction resistance changes only a few percent after being exposed to air for a week. Several junctions are made on the same a-InO_x strip to check the reproducibility of the junctions, which is very good. The normalized conductances, $G_j(V)/G_j(V=0)$, of all junctions on a single film agree within a percent.

We make our films following the technique described by Fiory and Hebard.[19] Hebard and Nakahara[20] have examined the microstructure of such films and find them to be amorphous indium oxide with occasional small crystallites of In_2O_3. We believe that our films have a similar microstructure because their electrical properties are similar. Our films have a mean-field transition temperature T_{co} which decreases linearly with room temperature resistivity ρ_N^2, as seen by Hebard and Fiory[21] (Fig. 2). T_{co} is measured by fitting the conductivity above T_{co} to the formula of Aslamazov and Larkin[22] and from the critical current. Our T_{co}'s are a little larger than those of Hebard and Fiory, but this difference probably involves small substrate effects.[23]

The normal-state conductivity $\sigma(T)$ of our films shows a strong T dependence due to electron localization and electron-electron interactions. Like the films of Fiory and Hebard[19] ours have $\sigma(T)=\sigma(0)+\alpha T^{1/4}$ from near T_{co} to room temperature. The inset in Fig. 3 shows the trend that $\sigma(0)$, the conductivity extrapolated to $T=0$, goes to zero when T_{co} goes to zero. The linearity between $\sigma(0)$ and $\sigma(295)$ is also consistent with those of Hebard and Kotliar,[24] as shown in Fig. 3, except for the systematic shift of our data upward. Selected samples with $d=350$ Å are marked in the figure, showing that the disorder of the samples reported here is not very close to the metal-insulator transition which occurs for $\rho_N\approx6.6$ mΩ cm ($\sigma_c\approx150\ \Omega^{-1}\,cm^{-1}$). This value is 20% larger than the value 5.3 mΩ cm of Hebard and Kotliar.[24]

Hence we conclude that our films are amorphous com-

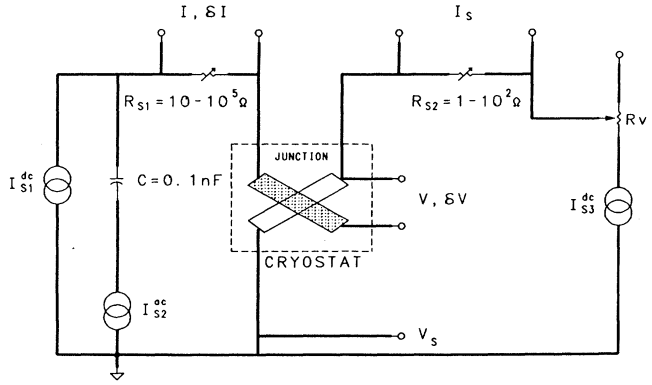

FIG. 1. Schematic sample configuration and wiring.

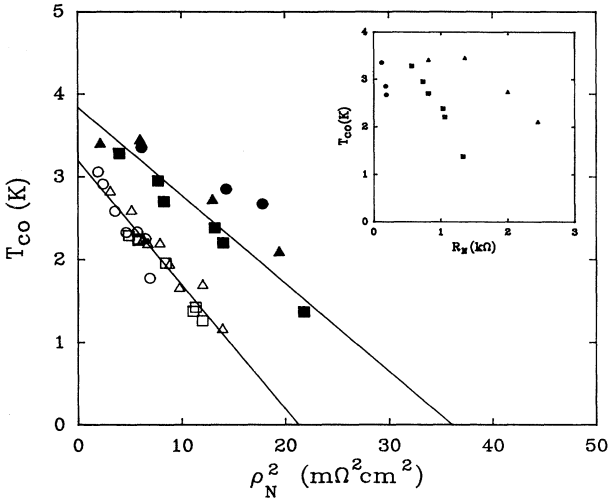

FIG. 2. Dependence of T_{co} on room-temperature resistivity ρ_N. Inset: T_{co} vs the corresponding room-temperature sheet resistance $R_\square$. Open symbols are from Ref. 21 and solid symbols are our data. The open circles, triangles, and squares correspond to film thicknesses 100, 200, and 400 Å, respectively. The filled circles, triangles, and squares are 2000, 180, and 350 Å.

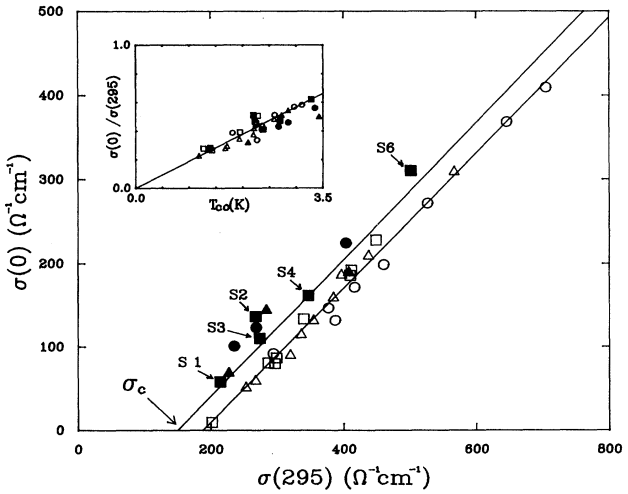

FIG. 3. Conductivity $\sigma(0)$ vs $\sigma(295$ K). Open symbols are from Ref. 24. Denotation of symbols is the same as Fig. 2. $\sigma_c\approx150\ \Omega^{-1}\,cm^{-1}$ marks the metal insulator transition. Inset: $\sigma(0)$ vs T_{co}.

TABLE I. Film thickness d, sheet resistance $R_\square$ (4.2 K), resistivity $\rho_{4.2}$, mean-field transition temperature T_{co}, zero-temperature order parameter $\Delta(0)$, fitted and calculated critical current $I_c(0)$. $N(0)\approx 1.7\times 10^{27}$ eV m^3 is calculated from $n\approx 4\times 10^{20}$ cm^{-3} (Ref. 19) for calculating $I_c(0)$.

Sample	d (Å)	$R_\square$ (kΩ)	$\rho_{4.2}$ (mΩ cm)	T_{co} (K)	$\Delta(0)$ (meV)	$I_c^{\rm fit}(0)$ (mA)	$I_c^{\rm cal}(0)$ (mA)	$\Delta(0)/k_B T_{co}$
1	350	2.80	9.8	1.37	0.30	4.2	4.0	2.55
2	350	1.74	6.0	2.20	0.41	9.2	8.4	2.18
3	350	1.60	5.6	2.38	0.45	11.4	9.6	2.18
4	350	1.16	4.0	2.60	0.53	16.0	14.5	2.35
5	375	0.88	3.3	2.95	0.59	23.3	20.1	2.30
6	350	0.68	2.4	3.28	0.63	33.5	24.5	2.23
7	180	1.00	1.8	3.37	0.65	16.7	15.1	2.24
8	840	0.17	1.4	3.77	0.67	119	86	2.07

posite, based on the all these data which show similar electrical transport properties to previous studies (Figs. 2 and 3). Furthermore, we emphasize that broadening of the resistive transition below T_{co} observed on these films is well explained with a Kosterlitz-Thouless type of phase transition without attributing it to inhomogeneity.[25,26] Reasons why we believe that inhomogeneities are unimportant are discussed in Ref. 1.

Sample parameters, measured directly or obtained from fits to tunneling data, are listed in Table I.

B. Measurement technique

A conventional four-terminal ac modulation technique is used for measuring the dynamic conductance $G_j(V,T)\equiv \partial I/\partial V|_T$ and the current voltage characteristic $I(V)$ of the junctions. The operating frequency is 100 Hz and the voltage resolution is about 10 nV. All the data are acquired by a computer-controlled system. Measurement is done with a ^{3}He probe between 0.5 and 1.3 K, and with an immersion-type ^{4}He probe above 1.2 K. The effect of the geomagnetic field is checked by doing the same measurements with a Dewar protected by dual-layered μ-metal shield (maximum ambient field inside the Dewar is less than 10 mG). No quantitative difference is found when compared to the data obtained without the shield.

The change in the junction conductance δG_j induced by a supercurrent in the a-InO_x film is measured as a function of supercurrent I_s at a given temperature and dc junction current I. Using a wiring scheme depicted in Fig. 1, the dc and ac junction currents are fixed and the change in ac junction voltage δV is monitored as I_s is swept from zero to nearly the critical current. δV is always kept small enough that instrumental smearing is negligible.

The supercurrent applied along the a-InO_x films is uniform across the film thickness d and width of the junction, since the magnetic penetration depth $\lambda\approx 2$ μm is much greater than film thicknesses ($d<1000$ Å), and the measured perpendicular magnetic penetration depth $\lambda_p=\lambda^2/d$ is on the order of millimeters,[27] and the film width is about 1 mm.

$\delta G_j \propto I_s^2$ is observed even when I_s is large enough to induce a slight voltage in the a-InO_x strip, so long as the slight voltage is small enough that it does not affect the current distribution through the junction. Very near the critical current, the voltage increases rapidly and limits the useful current range. Specifically, the dynamic sheet resistance of a-InO_x films at I_s up to about 80% of the directly measured critical current is less than 10 mΩ, which is 6 orders of magnitude smaller than the junction resistance. For stability, a Keithley 220 programmable source and mercury batteries are used for the sources of dc junction current and I_s, respectively.

Care is taken to avoid effects of heat dissipation from the resistive InO_x strip for I_s near I_c when the ^{3}He probe is used. This is checked by monitoring the drift in T of the sample while ramping I_s up to near I_c, after T was regulated at a certain value with $I_s=0$. From this procedure, we set a limit on I_s, which turns out to be about $0.7I_c(T)$.

There is a nontrivial technical issue that makes it attractive to measure δG_j vs I_s at fixed junction current I rather than voltage V. Since the dependence of V on I depends on I_s, and the junction is current biased, a feedback circuit for I could in principle keep V constant as I_s is varied. This is not possible when the supercurrent induces a voltage in the strip because then the measured dc voltage is the junction voltage V plus the voltage in the half of the a-InO_x strip in the voltage-measuring circuit (see Fig. 1). Rather than restrict our measurements to $I_s \ll I_c$, where a feedback circuit could be used, we measure at fixed I. Note that the measured ac voltage, which is proportional to δG_j, is unaffected by a slight dc voltage in the film because the ac voltage is measured in a true four-terminal way. Conversion of δG_j measured at fixed I to δG_j at fixed V is described in the Appendix. For simplicity, in the rest of the text, δG_j means δG_j at fixed voltage V.

III. THEORETICAL MODEL

To illustrate the effects of disorder qualitatively and to motivate our experimental method, Fig. 4 shows $G_j(V)$ measured at the same reduced temperature, $T/T_{co}=0.38$, for samples 1, 3, and 6. As ρ increases, the suppression of the normal-state density of states $N_n(E)$ at E_F grows and results in a severe deformation of the fa-

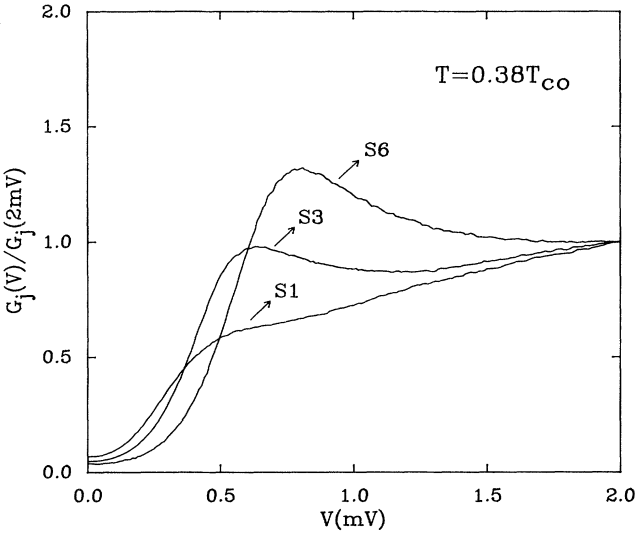

FIG. 4. $G_j(V)/G_j(2\text{ mV})$ vs V for samples 1, 3, and 6 at $T/T_{co}=0.38$.

miliar horn-shaped superconducting structure observed in conventional superconductors. It is not possible with sufficient accuracy to estimate $N_n(E)$ below T_{co} and below 2 mV by extrapolation of the measured $N_n(E)$ from either $T>T_{co}$ or $V>2$ mV because of the anomalous energy dependence of $N_n(E)$ (Ref. 16) and because of its strong temperature dependence (Fig. 5), which is stronger than that observed for a disordered normal metal, Ag.[28] Thus, we are led to our more complicated procedure which requires the following model to obtain the important parameters $1/\tau_{in}$, Δ, and $I_c(0)$.

We assume that the electron density of states per unit volume, $N_s(E)$, below T_{co} is the product of a dimensionless superconducting density of states $N_1(E)$, similar to the familiar BCS form, and the disorder-suppressed $N_n(E)$, so that $G_j(V,T)$ is given by

$$G_j(V)=C\int_{-\infty}^{\infty} dE\, N_1(E)N_n(E)\left[\frac{-\partial f(E-eV)}{\partial E}\right], \quad (1)$$

where $f(E)$ is the Fermi function and C is a constant proportional to the tunneling probability of electrons through the insulating barrier.[29,30] For all voltages for T near T_{co}, or for high voltages eV $\gg\Delta$ at any T, superconducting effects are small, so $N_1(E)\approx 1$ and $G_j(\text{eV})$ is a thermally smeared image of $N_n(E)$.

Our goal is to normalize $N_n(E)$ out of $N_s(E)$ with data from the same T where G_j is measured rather than from T near T_{co}. When a supercurrent is applied in the a-InO_x film, the superconducting density of states, $N_1(E)$, changes by δN_1 and results in a change δG_j in G_j. From Eq. (1), we have

$$\frac{\delta G_j}{G_j}=\frac{\int dE\,\delta N_1(E)N_n(E)[-\partial f(E-eV)/\partial E]}{\int dE\,N_1(E)N_n(E)[-\partial f(E-eV)/\partial E]} \quad (2)$$

$$\approx\frac{\int dE\,\delta N_1(E)[-\partial f(E)/\delta E|_{E-eV}]}{\int dE\,N_1(E)[-\partial f(E)/\partial E|_{E-eV}]}, \quad (3)$$

The step from Eq. (2) to (3) is quite accurate, based on numerical calculations with a reasonable estimate of $N_n(E)$ taken from $G_j(V)|_{T\approx T_{co}}$. Equation (3) shows that $N_n(E)$ is eliminated from $\delta G_j/G_j$ at any temperature.

A reasonable approach to modeling $\delta G_j/G_j$ would be to use the Eliashberg equations[31] to calculate $N_1(E)$ and Δ and adjust the coupling function $\alpha^2F(\omega)$ and pseudopotential μ^* to get the best fit to $\delta G_j/G_j$. This would enable us to obtain microscopic information from the phonon structure seen in the data. However, the solution of the Eliashberg equations for the density of states is very difficult except near $T=0$ and $T=T_{co}$. Instead, we use Beyer-Nielsen's weak coupling approximation[32] to the Eliashberg equations. In this approximation, Δ is independent of energy, and the effects of elastic and inelastic pairbreaking are included through the energy-independent normalized rates $\Gamma_s\equiv\hbar/\tau_s\Delta$ and $\Gamma_{in}\equiv\hbar/2\tau_{in}\Delta$. For $\Gamma_{in}=0$, the model reproduces Maki's dirty-limit theory[33] for the effect of a supercurrent on $N_1(E)$. In the other limit, $\Gamma_s=0$, the model yields Dynes's empirical approximation

$$N_1(E)\approx\text{Re}\{(E+i\hbar/2\tau_{in})/[(E+i\hbar/2\tau_{in})^2-\Delta^2]^{1/2}\},$$

which successfully models inelastic scattering effects on $N_1(E)$ in Pb-Bi,[34] a well-understood superconductor. Thus, the model serves as an interpolation between these two limits. The model[35] was used successfully in the analysis of nonequilibrium quasiparticle charge-imbalance relaxation measurements made via low-resistance junctions on Sn and SnIn films by Yen and Lemberger,[36] and on weakly disordered Al films by Lee and Lemberger.[3] The model also describes measurements

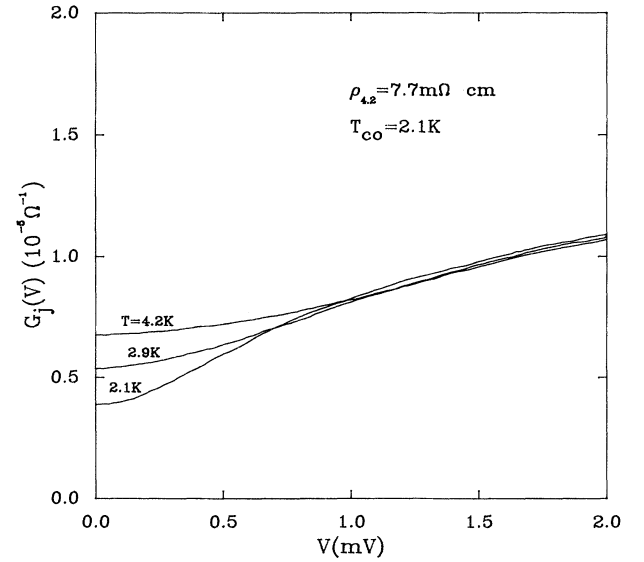

FIG. 5. $G_j(V)$ vs V at $T=4.2$, 2.9, and 2.1 K. $\rho_{4.2}$ of the InO_x film is 7.7 mΩ cm; $T_{co}=2.1$ K. Strong T dependence of $G_j(V)$ for $V<1$ mV is evident.

on higher-resistance junctions on Sn and Al in which nonequilibrium effects were negligible.[37] In all of these measurements, a supercurrent was used to modulate the resistance of the junction.

In the present work, elastic pair breaking has two origins; one ($1/\tau_{s,\text{ext}}$) comes from the externally applied supercurrent, and the other ($1/\tau_{s,\text{int}}$) from thermal phase fluctuations,[3] which are intrinsic and discussed in the next section. $1/\tau_{s,\text{ext}}$ is related to the supercurrent I_s through[3,33]

$$\hbar/\tau_{s,\text{ext}} = Dp_s^2/2\hbar = 0.167(k_B T_{co})[n_s(0)/n_s(T)]^2[I_s/I_c(0)]^2 , \quad (4)$$

where

$$I_c(0)^2 = (0.467)2N(0)\Delta(0)^3(dw)^2/\hbar\rho_{4.2} . \quad (5)$$

$I_c(0)$ is the zero-temperature depairing critical current, D is the electron diffusion constant, $p_s = 2mv_s$ is the superfluid momentum, and n_s is the density of superconducting electrons. The free-electron relation $1/\rho = 2N(0)e^2D$ is used in Eqs. (4) and (5). Table I shows the good agreement between the fitted values of $I_c(0)$ and values from Eq. (5), even though Eq. (5) does not include effects of strong disorder.

The theoretical model actually yields N_1 as a function of E/Δ for given Γ_s and Γ_{in}, that is, it yields the shape of the density of states. The change, $\delta N_1(E)$, as a function of absolute energy E, is calculated from

$$\delta N_1(E/\Delta) \equiv N_1[E/\Delta(I_s), I_s] - N_1[E/\Delta(0), I_s = 0] ,$$

taking into account that Δ is a function of I_s, i.e., $1/\tau_{s,\text{ext}}$. We use Maki's theory[33] to calculate $\Delta(1/\tau_{s,\text{ext}})$, since for our samples inelastic scattering is relatively weak, $\Gamma_{\text{in}} < 0.1$, and Maki's theory obtains for $\Gamma_{\text{in}} = 0$.

For illustration, Fig. 6 shows the dependence of N_1 on E/Δ (solid lines), calculated for two cases: (1) no pair breaking, $\Gamma_{\text{in}} = \Gamma_{s,\text{int}} = \Gamma_{s,\text{ext}} = 0$ (BCS), and (2) weak inelastic pair breaking, $\Gamma_{\text{in}} = 0.1$, $\Gamma_{s,\text{int}} = \Gamma_{s,\text{ext}} = 0$. The dotted lines show the effect of a small supercurrent corresponding to $\Gamma_{s,\text{ext}} = 0.02$. Inset shows the change $\delta N_1(E/\Delta)$ caused by a supercurrent (not including the effect of current on Δ for simplicity). Note that the effect of the supercurrent is to move N_1 toward its normal-state value of unity, so it increases N_1 for $E < \Delta$, where N_1 is less than unity, and it decreases N_1 for $E > \Delta$, where N_1 is greater than unity.

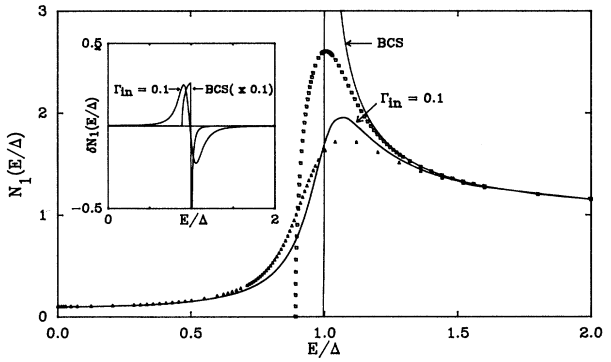

FIG. 6. The calculated $N_1(E/\Delta)$ vs E/Δ for BCS case ($\Gamma_{\text{in}} = 0$) and for $\Gamma_{\text{in}} = 0.1$. Dotted curves show the effect of supercurrent ($\Gamma_{s,\text{ext}} = 0.02$). Inset: $\delta N_1(E/\Delta) = N_1(E/\Delta, I_s) - N_1(E/\Delta, I_s = 0)$ for the same cases.

Figure 7 shows $\delta G_j/G_j$ calculated as a function of bias voltage for three different cases: (1) no pair breaking ($\Gamma_{\text{in}} = \Gamma_{s,\text{int}} = 0$), (2) weak intrinsic elastic pair breaking ($\Gamma_{s,\text{int}} = 0.1$; $\Gamma_{\text{in}} = 0$), and (3) weak inelastic pair breaking ($\Gamma_{s,\text{int}} = 0$, $\Gamma_{\text{in}} = 0.1$). Comparison of these cases suggests that gaplessness in the density of states [case (3)] is responsible for the minimum at $eV = 0$. Furthermore, we see that intrinsic elastic pairbreaking $\Gamma_{s,\text{int}}$, which broadens the peak but does not produce a low-energy tail in N_1, has a relatively minor effect on $\delta G_j/G_j$, at least for $\Gamma_{s,\text{int}} < 0.1$. We estimate for our films a largest value for $\Gamma_{s,\text{int}}$ of about 0.1 from the experimental result[3] $1/\tau_{s,\text{int}} \approx 2.2 \times 10^7 R_\square T\,\text{s}^{-1}$, with $R_\square \approx 1000\ \Omega$, a typical highest T of 2 K, and a typical measured Δ of about $2.3kT_{co}$. Thus, we are unable to determine $\Gamma_{s,\text{int}}$ from our data, and we neglect it in the analysis.

The features of $\delta G_j/G_j|_V$ seen in Fig. 7 can be explained as follows. $\delta G_j(V)$ is a thermally broadened $\delta N_1(eV)$. Since the supercurrent has its largest effect on states near Δ, δN_1 is largest just above and below Δ and decreases rapidly as $V \to 0$ (see Fig. 6). Numerical calculations show little difference among $\delta G_j(V)$ for the three cases mentioned above. However, $G_j(V)$ is very different if inelastic scattering is present. Near $V = 0$, G_j is greatly increased by a low-energy tail in N_1 caused by inelastic scattering. Thus, $\delta G_j/G_j$ at $V = 0$ is much smaller when inelastic scattering exists. When V increases to about $(\Delta - kT)/e$, then electrons can tunnel into the large number of states near $E = \Delta$ and the tail becomes unimportant, so G_j is roughly the same for all cases and the different curves for $\delta G_j/G_j$ merge. The conclusion is

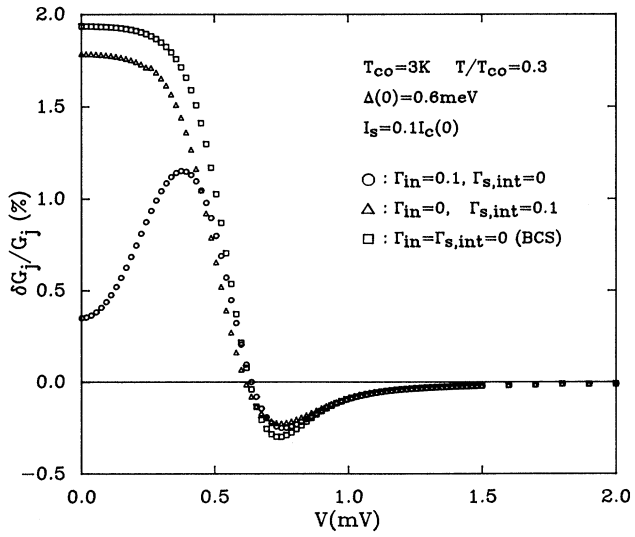

FIG. 7. Calculated $\delta G_j/G_j|_V$ vs V in three different cases (see text).

that measurements of $\delta G_j/G_j|_V$ allow us to divide out $N_n(E)$ and thereby obtain $N_1(E)$, and they provide a clear feature which allows us to extract an effective $1/\tau_{in}$ as a function of T.

IV. EXPERIMENTAL RESULTS AND DISCUSSION

We begin with the conductance $G_j(V)$ of sample 3 at several different temperatures, (Fig. 8). The inelastic tail in N_1 is evident from the zero-bias conductance, which is 20 times larger than BCS for $\Delta=0.45$ meV. We tried to obtain values of $1/\tau_{in}$ by fitting $G_j(V,T)/G_j(V,T_{co})$ vs V, but were unable to get good fits. Rough estimates of $1/\tau_{in}$ from the temperature dependence of the zero-bias conductance $G_j(V=0,T)$ are roughly four times those from fits to $\delta G_j/G_j$.[17]

Finally, we move on to fit $\delta G_j/G_j$. $\delta G_j/G_j$ shows the expected minimum at $V=0$, as shown in Fig. 9 for sample 3. Solid curves are calculated for various values of Γ_{in}. The fitting procedure is first to estimate Δ from the point where $\delta G_j/G_j$ reverses sign. Next, adjust Γ_{in} to fit the shape of $\delta G_j/G_j$ below $V\approx\Delta/e$. Finally, adjust $I_c(0)$ to get the magnitude of $\delta G_j/G_j$ right. Δ, Γ_{in}, and $I_c(0)$ are nearly independent fitting parameters.

Values of the fitting parameters Δ and $I_c(0)$ are reasonable. $\Delta(T)/\Delta(0)$ has the expected BCS form (Fig. 10), and $\Delta(0)/kT_{co}$ has a typical strong-coupling value of about 2.3, as is common in amorphous metals.[38] A single value of $I_c(0)$ fits the data on a given sample at all temperatures, which means that $n_s(T)$ [Eq. (4)] has the usual dirty-limit T dependence. Fitted values of $I_c(0)$ agree well with values calculated from Eq. (5). By using the measured $\Delta(0)$ in Eq. (5), we account roughly for strong coupling, but a better comparison with theory is needed. Apparently strong disorder does not have a strong effect on $I_c(0)$ despite the large suppression in $N_n(E)$ near E_F. See Table I for the numbers.

The minimum in $\delta G_j/G_j$ at $V=0$ is observed to disappear for $T>0.6T_{co}$ because tunneling of thermally excited quasiparticles into the peak in $N_1(E)$ makes the tail in N_1 irrelevant at all bias voltages. Within our model, we find that the minimum vanishes when $T>0.6T_{co}$, regardless of the magnitude of Γ_{in}.

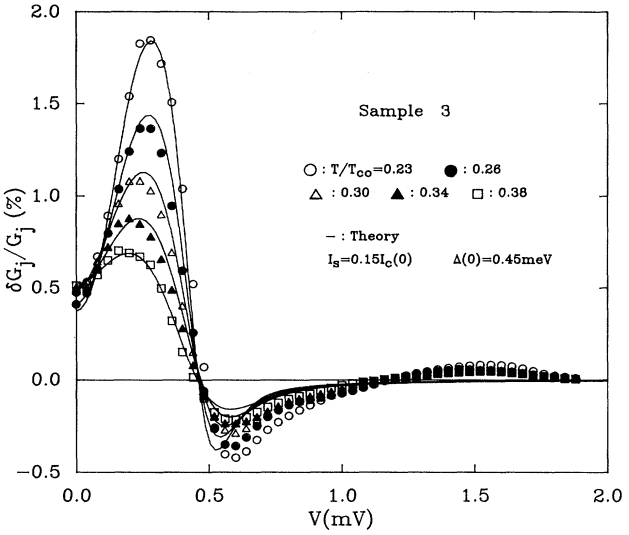

FIG. 9. $\delta G_j/G_j|_V$ vs V for sample 3 for several temperatures.

The quality of the fits to $\delta G_j/G_j$ for all samples is comparable to that shown in Fig. 9, where the fits are quite good below about 0.5 mV. Above 0.5 mV the model deviates from the data. In particular, there is another sign reversal in the data at about 1.2 mV. As discussed in Ref. 1, this discrepancy probably arises from a strong phonon mode at about 0.7 mV, which increases $N_1(E)$ for $E\leq\Delta+0.7$ meV ≈ 1.1 meV and reduces $N_1(E)$ below unity for $E\geq 1.1$ meV, so that the measured conductance above 1.1 mV is lower than the normal-state conduc-

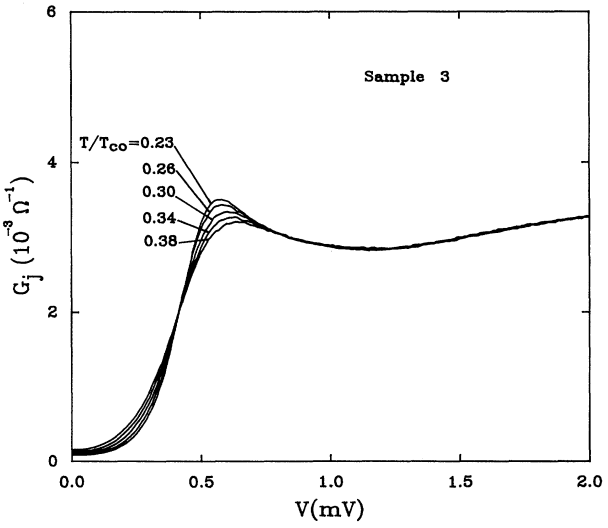

FIG. 8. $G_j(V)$ vs V for sample 3 for several temperatures.

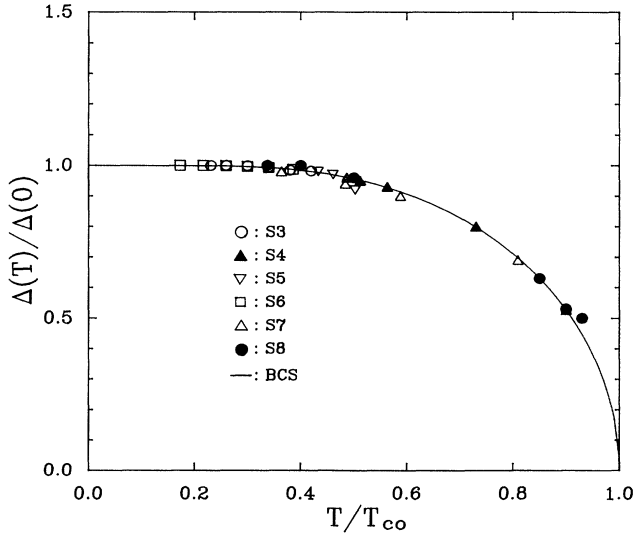

FIG. 10. Measured gap $\Delta(T)/\Delta(0)$ vs T.

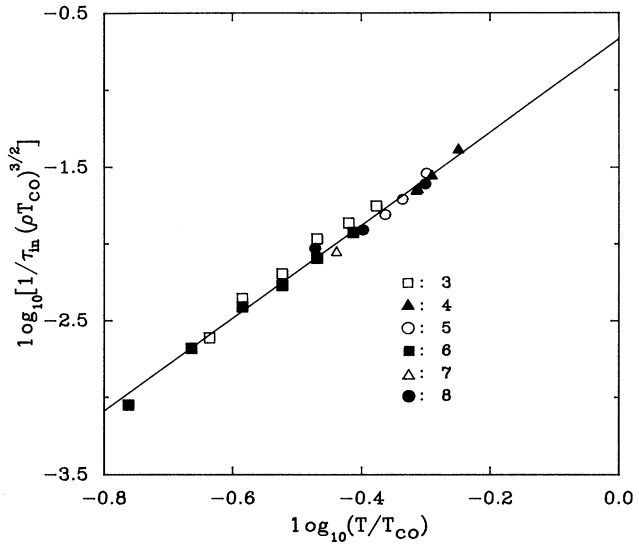

FIG. 11. Inelastic scattering rate $1/\tau_{in}$ normalized by $(\rho_{4.2}T_{co})^{3/2}$ as a function of T/T_{co} in log-log scale. $1/\tau_{in}$ is in units of kelvin.

tance.[31] Thus, the supercurrent raises the conductance toward its normal state value for $V \geq 1.1$ mV and $\delta G_j/G_j$ is positive again. It will be interesting to reexamine this feature when the theory can calculate the tunneling conductance directly, including disorder and strong coupling.

We note that a strong-coupling modification of the density of states so close to $E=\Delta$ could be the reason that we were unable to fit the peak in $G_j(V,T)/G_j(V,T_{co})$ vs V with our model, which does not include such strong coupling features because it neglects the energy dependences of $1/\tau_{in}$ and Δ.

The main result of this study is that

$$1/\tau_{in} \approx 2.8\times 10^{10}\ \mathrm{s}^{-1}[\rho_{4.2}[\mathrm{m}\Omega\,\mathrm{cm}) T_{co}(K)]^{3/2}(T/T_{co})^3 ,$$

with surprisingly little scatter. Figure 11 shows $1/\tau_{in}$ normalized to $(\rho_{4.2}T_{co})^{3/2}$ plotted vs T/T_{co} on a log-log scale. Samples 3 and 6 were reported in Ref. 1. The solid line has a slope of 3. The scaling with $\rho_{4.2}$ rather than $R_\square = \rho_{4.2}/d$ indicates that the inelastic scattering is 3D in nature, rather than 2D. Devereaux and Belitz[14,15] find that the imaginary part of the electron self-energy agrees well with our inelastic rate. They find that our 180-Å-thick films are just approaching the dimensional crossover from 3D to 2D.

V. CONCLUSION

We have performed tunneling measurements on high-resistance Al/AlO_x/a-InO_x junctions as a function of bias voltage V, temperature T, and supercurrent I_s to study the effects of disorder on superconductivity for $T \ll T_{co}$.

Measurements of the fractional change in junction conductance caused by a supercurrent applied to the a-InO_x film enable separation of the disorder dependence of the superconducting and normal electron densities of states. The data for $\delta G_j/G_j$ vs V reveal inelastic broadening in the superconducting density of states as a minimum at $V=0$ and strong electron-phonon coupling as a second zero crossing just above 1 meV. Both of these features are obscured by the normal background in the conductance trace, $G_j(V)$ vs V.

By interpreting the data with a semiphenomenological model, we obtain an effective inelastic scattering rate $1/\tau_{in}$ as a function of temperature and disorder. The observed rate is proportional to $(T/T_{co})^3$ even for $T \ll T_{co}$, where $\hbar/\tau_{in}\Delta \ll 1$. A theory for the electron self-energy of disordered superconductors, including the correlation gap contribution, at $T/\Delta \ll 1$ describes the dependence of the measured rate on temperature and on disorder, i.e., resistivity.[15]

$\Delta(0)/kT_{co}$ is roughly constant as $T_{co} \to 0$, as is observed for uniform quench-condensed Pb films but not for uniform quench-condensed Sn films.[39] The fitted critical current at $T=0$, $I_c(0)$, is not affected much by strong disorder.

There is much more that needs to be done. First, measurements are needed on other materials, preferably materials with a microstructure different from that of a-InO_x. Data are needed on thinner films to see the crossover from 3D to 2D predicted by theory. A technique needs to be found to look for the effects of thermal phase fluctuations in strongly disordered superconductors, which the current experimental technique does not see. These fluctuations should contribute to broadening of the peak in $N_1(E)$.

A rigorous comparison between theory and experiment will be possible when theory can calculate the measured quantities, namely, the junction conductance $G_j(V)$ and the change $\delta G_j(V)$ induced by a supercurrent in the film. Also, theory likely needs to include thermal phase fluctuations, especially in 2D, since the effective pair-breaking rate is linear in T and other processes which broaden the peak in $N_1(E)$ decrease more rapidly.

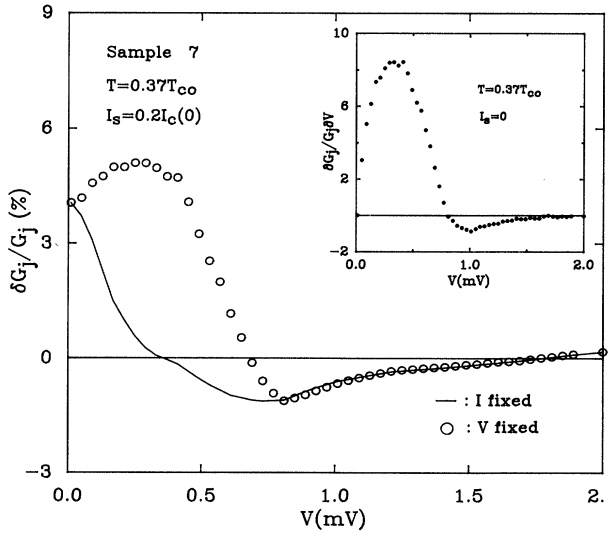

FIG. 12. Measured $\delta G_j/G_j|_I$ vs V (solid line) and $\delta G_j/G_j|_V$ vs V (circles) for sample 7. Inset shows $(1/G_j)\partial G_j/\partial V$ vs V.

ACKNOWLEDGMENTS

We have benefited from discussions with Dietrich Belitz, Thomas Devereaux, Liam Coffey, and Arthur Hebard. These results are based on work supported by the Low-Temperature Physics Program of the National Science Foundation under Grant Nos. DMR 85-15370 and 88-22242. We are grateful for the use of facilities of the Ohio State University Center for Materials Research.

APPENDIX

The important quantity is the change in conductance at fixed voltage,

$$\delta G_j(V,T,I_s) \equiv G_j(V,T,I_s) - G_j(V,T,0) .$$

It is straightforward to obtain $\delta G_j(V,T,I_s)$ at fixed voltage from the measured δG_j, taken at fixed current I, and $G_j(V,T)$.[17] The key relation is

$$\left.\frac{\partial G_j}{\partial (I_s^2)}\right|_{V,I_s=0} = \left.\frac{\partial G_j}{\partial (I_s^2)}\right|_{I,I_s=0} + \left.\frac{\partial G_j}{\partial V}\right|_{I_s=0} \times \int_0^V dV' \frac{1}{G_j(V')} \left.\frac{\partial G_j}{\partial (I_s^2)}\right|_{I,I_s=0} , \quad \text{(A1)}$$

where measured values for G_j and its derivatives are used on the right-hand side. We have checked this result numerically. We obtain $\delta G_j/G_j|_V$ at a given I_s by multiplying $\partial G_j/\partial (I_s^2)|_{V,I_s=0}$, by I_s^2 and then dividing by $G_j(V,I_s=0)$. For reference, Fig. 12 shows the raw data, $\delta G_j/G_j|_I$, the calculated quantity $\delta G_j/G_j|_V$, and $(\partial G_j/G_j)/\partial V|_{I_s=0}$ (inset) calculated numerically from the measured $G_j(V)$, all for sample 7 at $T/T_{co}=0.37$.

[1] D. S. Pyun and T. R. Lemberger, Phys. Rev. B **34**, 3732 (1991).
[2] T. P. Deveraux and D. Belitz, J. Low Temp. Phys. **77**, 319 (1989).
[3] S. G. Lee and T. R. Lemberger, Phys. Rev. B **40**, 10 831 (1989).
[4] R. P. Peters and G. Bergmann, J. Phys. Soc. Jpn. **54**, 3478 (1985).
[5] P. Santhanam, S. Wind, and D. E. Prober, Phys. Rev. B **35**, 3188 (1987).
[6] K. C. Mui, P. Lindenfeld, and W. L. McLean, Phys. Rev. B **30**, 2951 (1984).
[7] P. C. van Son, J. Romijn, T. M. Klapwijk and J. E. Mooij, Phys. Rev. B **29**, 1503 (1984).
[8] T. M. Klapwijk, P. A. van der Plas, and J. E. Mooij, Phys. Rev. B **33**, 1474 (1986).
[9] D. Belitz and S. Das Sarma, Phys. Rev. B **36**, 7701 (1987).
[10] D. Belitz and K. I. Wysokinski, Phys. Rev. B **36**, 9333 (1987).
[11] M. Yu. Reizer and A. V. Sergeyev, Zh. Eksp. Teor. Phys. **90**, 1056 (1986). [Sov. Phys. JETP **63**, 616 (1986)].
[12] B. I. Altshuler and A. G. Aronov, in *Electron-Electron Interactions in Disordered Systems,* edited by A. L. Efros and M. Pollack (North-Holland, New York, 1985).
[13] A Schmid, Z. Phys. **271**, 251 (1974).
[14] T. P. Devereaux and D. Belitz, Phys. Rev. B **34**, 3736 (1991).
[15] T. P. Devereaux and D. Belitz (unpublished).
[16] D. S. Pyun and T. R. Lemberger, Phys. Rev. Lett. **63**, 2132, (1989).
[17] D. S. Pyun, Ph.D. thesis, Ohio State University, 1990 (unpublished).
[18] J. M. Vandenberg, S. Nakahara, and A. F. Hebard, J. Vac. Sci. Technol. **18**, 268 (1981).
[19] A. T. Fiory and A. F. Hebard, Phys. Rev. Lett. **52**, 2057 (1984).
[20] A. F. Hebard and S. Nakahara, Appl. Phys. Lett. **41**, 1130 (1982).
[21] A. F. Hebard and A. T. Fiory, Phys. Rev. Lett. **58**, 1131 (1987).
[22] L. G. Aslamazov and A. I. Larkin, Phys. Lett. **26A**, 238 (1968).
[23] A. F. Hebard and A. T. Fiory, in *Novel Superconductivity,* editd by S. A. Wolf and V. Z. Kresin (Plenum, New York, 1987).
[24] A. F. Hebard and G. Kotliar, Phys. Rev. B **39**, 4105 (1989).
[25] A. F. Hebard and A. T. Fiory, Phys. Rev. Lett. **50**, 1603 (1983).
[26] A. T. Fiory, A. F. Hebard, and W. I. Glaberson, Phys. Rev. B **28**, 5075 (1983).
[27] D. S. Pyun, E. R. Ulm, and T. R. Lemberger, Phys. Rev. B **39**, 4140 (1989).
[28] J. M. Valles, R. C. Dynes, and J. P. Garno, Phys. Rev. B **40**, 7590 (1989).
[29] W. L. McMillan and J. M. Rowell, in *Superconductivity,* edited by R. D. Parks, (Marcel Dekker, New York, 1969), Vol. 1.
[30] M. Tinkham, *Introduction to Superconductivity* (McGraw-Hill, New York, 1975).
[31] D. J. Scalapino, in *Superconductivity* (Ref. 29).
[32] J. Beyer-Nielsen *et al.*, J. Low Temp. Phys. **46**, 565 (1982); J. Beyer-Nielsen, Ph.D. thesis, H. C. Oersted Institute, 1983 (unpublished).
[33] K. Maki, in *Superconductivity,* edited by R. D. Parks (Marcel Dekker, New York, 1969), Vol. 2.
[34] R. C. Dynes, V. Narayanamurti, and J. P. Garno, Phys. Rev. Lett. **41**, 1509 (1978).
[35] T. R. Lemberger, Y. Yen, and S. G. Lee, Phys. Rev. B **35**, 6670 (1987).
[36] Y. Yen and T. R. Lemberger, Phys. Rev. B **37**, 3324 (1988).
[37] Y. Yen, S. G. Lee, and T. R. Lemberger, Phys. Rev. B **36**, 8408 (1987).
[38] G. Bergmann, Phys. Rep. **27**, 159 (1976).
[39] J. M. Valles, R. C. Dynes, and J. P. Garno, Phys. Rev. B **40**, 6680 (1989).